Published OnlineFirst March 3, 2020; DOI: 10.1158/1535-7163.MCT-19-0461

Identification of ALDH1A3 as a Viable Therapeutic Target in Breast Cancer Metastasis–Initiating Cells

Daisuke Yamashita[1], Mutsuko Minata[1], Ahmed N. Ibrahim[1], Shinobu Yamaguchi[1], Vito Coviello[2], Joshua D. Bernstock[3], Shuko Harada[4], Richard A. Cerione[5], Bakhos A. Tannous[6], Concettina La Motta[2], and Ichiro Nakano[1,7]

ABSTRACT

The development of efficacious therapies targeting metastatic spread of breast cancer to the brain represents an unmet clinical need. Accordingly, an improved understanding of the molecular underpinnings of central nervous system spread and progression of breast cancer brain metastases (BCBM) is required. In this study, the clinical burden of disease in BCBM was investigated, as well as the role of aldehyde dehydrogenase 1A3 (ALDH1A3) in the metastatic cascade leading to BCBM development. Initial analysis of clinical survival trends for breast cancer and BCBM determined improvement of breast cancer survival rates; however, this has failed to positively affect the prognostic milestones of triple-negative breast cancer (TNBC) brain metastases (BM). ALDH1A3 and a representative epithelial–mesenchymal transition (EMT) gene signature (mesenchymal markers, CD44 or Vimentin) were compared in tumors derived from BM, lung metastases (LM), or bone metastases (BoM) of patients as well as mice after injection of TNBC cells. Selective elevation of the EMT signature and ALDH1A3 were observed in BM, unlike LM and BoM, especially in the tumor edge. Furthermore, ALDH1A3 was determined to play a role in BCBM establishment via regulation of circulating tumor cell adhesion and migration phases in the BCBM cascade. Validation through genetic and pharmacologic inhibition of ALDH1A3 via lentiviral shRNA knockdown and a novel small-molecule inhibitor demonstrated selective inhibition of BCBM formation with prolonged survival of tumor-bearing mice. Given the survival benefits via targeting ALDH1A3, it may prove an effective therapeutic strategy for BCBM prevention and/or treatment.

Introduction

Globally, breast cancer is the most frequently diagnosed cancer and the leading cause of cancer mortality in women; ultimately approximately 12% of women within the United States will be diagnosed over the course of their lifetimes (1). Breast cancer brain metastases (BCBM) represent a late stage in breast cancer progression; current therapeutic options demonstrate limited efficacy resulting in overall survival (OS) on the order of months (1, 2). The incidence of BCBM continues to increase, due in part to improved management of primary breast cancer and subsequent prolongation of survival (1, 2). Unfortunately, recently developed targeted therapies that control primary disease in breast cancer have diminished efficacy against metastatic brain lesions (1, 2). It is also prudent to note that disparities exist in the prognostication of breast cancer with regard to tumor receptor positivity [i.e., $HER2^+$, estrogen (ER^+), and progesterone (PR^+); ref. 1]. Inherently, triple-negative breast cancer (TNBC) more frequently progresses to BM as compared with other breast cancer subtypes and is associated with an extremely poor prognosis following BCBM establishment (3–5).

Although the precise governing biology of BCBM remains to be fully elucidated, previous studies have demonstrated the existence of molecular signatures distinct to tumors which have metastasized to and ultimately colonized the brain (6–9). However, these advances have failed to translate to actionable biomarkers and/or molecular targeted therapies for BCBM (10). The poor prognosis also relates to BCBM cell's aggressive proliferation compared with breast cancer cells that colonize other organs (e.g., lung, bone, etc.; refs. 11, 12), suggesting that breast cancer cells acquire brain-primed properties potentially via bidirectional interplay with the blood–brain barrier (BBB) and/or brain microenvironment. Previous genomic characterization of BM has demonstrated that metastatic and primary tumors share a common ancestor, yet continue to evolve independently (i.e., branched evolution; ref. 13). Interestingly, those findings also suggested that clinically actionable alterations present in BCBM are often absent in primary breast biopsies (13).

The establishment of BM has been described as a cascade involving primary breast cancer cell invasion into feeding vessels, dissemination/survival through the circulatory system, adhesion to brain vascular endothelial cells, and extravasation for colonization and ultimately propagation within the brain (14, 15). Arrest of circulating tumor cells (CTC) at branches of capillaries denotes the first step in the transmigration process (16). Active adhesion between CTCs and the vascular wall is required for efficient extravasation, though narrow capillary size alone is capable of ensnaring CTCs (17). Following adhesion, extravasation of CTCs involves massive endothelial remodeling with encapsulation of single cells or clusters of arrested CTCs by the formation of

[1]Department of Neurosurgery, University of Alabama at Birmingham, Birmingham, Alabama. [2]Department of Pharmacy, University of Pisa, Pisa, Italy. [3]Department of Neurosurgery, Brigham and Women's Hospital, Harvard Medical School, Boston, Massachusetts. [4]Department of Pathology, University of Alabama at Birmingham, Birmingham, Alabama. [5]Department of Molecular Medicine VMC, Cornell University, Ithaca, New York. [6]Experimental Therapeutics and Molecular Imaging Lab, Department of Neurology, Neuro-oncology Division, Massachusetts General Hospital, Harvard Medical School, Boston, Massachusetts. [7]O'Neal Comprehensive Cancer Center, University of Alabama at Birmingham, Birmingham, Alabama.

Note: Supplementary data for this article are available at Molecular Cancer Therapeutics Online (http://mct.aacrjournals.org/).

D. Yamashita and M. Minata contributed equally to this article.

Corresponding Author: Ichiro Nakano, University of Alabama at Birmingham, 410F WTI UAB Comprehensive Cancer Center, Birmingham, AL 35243. Phone: 614-292-0358; Fax: 614-292-0358; E-mail: inakano@uabmc.edu

Mol Cancer Ther 2020;19:1134–47

doi: 10.1158/1535-7163.MCT-19-0461

Published OnlineFirst March 3, 2020; DOI: 10.1158/1535-7163.MCT-19-0461

endothelial domes (17). Finally, astrocytes produce inflammatory factors and support colonization/propagation via the activation of STAT1 and NF-κB pathways in BM cells (18).

Cancer stem cells (CSC) have been demonstrated to play a critical role in the initiation of metastasis, whereas other studies have suggested that ALDH-positive cells exhibit stem cell–like properties, thus indicating a potential role in metastatic cascade (19–21). Also, it has been reported that both $CD44^+/CD24^-$ and $ALDH1^+$ breast CSCs are enriched in TNBC and may contribute to chemotherapy resistance and tumor metastasis of TNBC (22, 23). Interestingly, our previous work in glioblastoma (GBM) has suggested that ALDH1A3 and CD44 expressions are correlated with the aggressive and radioresistant mesenchymal (MES) subtype as compared with the proneural (PN) subtype (24).

Herein, we sought to identify a novel molecular signature of BCBM in an effort to develop and ultimately engage therapeutic targets such as ALDH1A3. In so doing, we have demonstrated that ALD1A3 is involved in core aspects of BCBM and can be effectively engaged via a novel small-molecule inhibitor (i.e., MF-7).

Materials and Methods

Ethics

All work related to human tissue was performed at the University of Alabama at Birmingham (UAB) under an Institutional Review Board–approved protocol (N150219008) compliant with guidelines set forth by NIH. Patients gave informed, written consent for use of their tissues as appropriate in accordance with this permission, and the study protocol conformed to the Declaration of Helsinki. Patient-derived specimens were provided to the corresponding scientists after deidentification of the original tumors.

Drugs

The chemical structures of test compounds MF-7 and GA11are found in **Fig. 6**A. They were synthesized as outlined in Supplementary Fig. S1. The commercially available 5-bromopyridin-2-amine (1.00 mmol) was reacted with 2-bromo-1-phenylethan-1-one (1.20 mmol) and potassium carbonate (1.20 mmol) in refluxing ethanol to give the key intermediate 6-bromo-2-phenylimidazo[1,2-*a*]pyridine. Treatment of the intermediate (1.00 mmol) with the suitable phenylboronic acid (1.50 mmol), in the presence of Pd $(OAc)_2$ (0.10 mmol), PPh_3 (0.20 mmol), and 2 mL of Na_2CO_3 2M, in toluene solution, afforded the target inhibitors, MF7 and GA11. Crude compounds were purified by column chromatography (silica gel, ethyl acetate/petroleum ether), recrystallized from the suitable solvent, and characterized by physio-chemical and spectroscopic data (Supplementary Table S1).

Cell culture

MDA-MB-231 (MDA-231) cells were purchased from the ATCC, and MDA-MB-468 (MDA-468) cells were kindly provided by Dr. Amdra R. Frost (UAB). We established a metastatic murine model via the cardiac injection of MDA-MB-231 and MDA-MB-468 using immunocompromised mice (SCID Beige) and then produced a series of derivative cell lines from the resultant tumors within the brain (231-BM and 468-BM), lung (231-LM), or bone (231-BoM). These cells were grown in advanced RPMI 1640 medium (Gibco) supplemented with 1% penicillin/streptomycin, 10% FBS (Atlanta Biologics), and 100x L-glutamine (Gibco). HBEC cells were purchased from the ATCC and cultured in DMEM/F12 medium (Gibco) supplemented with endothelial cell growth factor (Millipore). Cell lines were screened for *Mycoplasma* every 4 months.

Plasmid transfection and lentiviral/retroviral transduction

Lentiviral vectors expressing shRNA for ALDH1A3 were purchased from Sigma. Lentiviruses were produced as has been previously described (25). Briefly, 293T cells (Invitrogen) were cotransfected with pLKO.1 vector encoding the shRNA and the helper plasmids for virus production (psPAX2 and pMGD2) using calcium phosphate (Clontech). Lentivirus was harvested at 72 hours after transfection and concentrated 100-fold using Lenti-X concentrator (Clontech). Viral transduction was performed with polybrene according to the manufacturer's protocol. shRNAs targeting ALDH1A3 were produced based on the following clones (Sigma) (shALDH1A3 clone 1: CCGGGCAACCA-ATACTGAAGTTCAA-CTCGAGTTGAACTTCAGTATTGGTTGCTTTTT; shALDH1A3 clone 2: CCGGGCCGAATACACAGAAGTGAAACTCGAGTTT CACTTCTGTGTATTCGGCTTTTT).

siRNA

One day before transfection, dissociated cells (4×10^5 cells) were plated in medium without antibiotics. After diluting lipofectamine RNAiMAX reagent in Opti-MEM medium (Gibco) and the desired concentration of siRNA (100 nmol/L) in Opti-MEM medium, both mixtures were combined (1:1 ratio) and incubated at room temperature (RT) for 5 minutes. The siRNA–lipid complex was added to each well and incubated for 6 hours. Experiments were performed 72 hours after transfection.

RNA isolation and qRT-PCR

Total RNA was extracted using RNeasy mini kit (Qiagen) as per the manufacturer's instructions. RNA concentration was determined using Nanodrop One (Thermo Scientific). cDNAs were synthesized using iScript reverse transcription supermix (Bio-Rad) according to the manufacturer's protocol. qRT-PCR was performed on StepOnePlus thermal cycler (Thermo scientific) with SYBR Select Master Mix (Thermo scientific). GAPDH was used as an internal control. Primer sequences are shown in Supplementary Table S2.

Western blotting

Western blotting (WB) was performed as has been previously described (26). Antibodies against ALDH1A3 (rabbit, Sigma), CD44 (mouse, Cell Signaling Technology), Vimentin (rabbit, Cell Signaling Technology), and β-actin (mouse, Cell Signaling Technology) were used. Staining was visualized with Amersham ECL Western Blot System (GE Healthcare).

IHC and immunofluorescence

IHC and immunofluorescence (IF) were performed as previously described (27). For IHC, signals were detected using the DAB substrate kit (Vector). For double staining, donkey IgG H&L (alkaline phosphatase) preadsorbed antibody (Abcam) was used for the targeted primary antibody as a secondary antibody and detected by the liquid fast-red substrate kit (Abcam). The primary antibodies used in this study were as follows: anti-CD44 (mouse, Cell Signaling Technology), anti-Vimentin (mouse, Cell Signaling Technology), and anti-ALDH1A3 (rabbit, Sigma). For IF, primary antibodies were visualized with Alexa Fluor 488 (green)– or 555 (red)–conjugated secondary antibodies (Cell Signaling Technology). Nuclei were counter-stained with Hoechst 33258 (Thermo Fisher).

Cell viability assay

Viability of GBM cells was determined using an AlamarBlue assay (Thermo Fisher Scientific). Briefly, cells were seeded at 3,000 cells per

Published OnlineFirst March 3, 2020; DOI: 10.1158/1535-7163.MCT-19-0461

well in a 96-well plates (excitation at 515–565 nm and emission at 570–610 nm were the parameters employed); a Synergy HTX multi-mode reader (BioTek) was utilized for all experiments.

Adhesion assay

Coverslips placed in a 24-well plate were coated with laminin (Sigma) diluted in PBS (1:100) for 3 hours. HBEC cells were then seeded on these coverslips and allowed to grow to approximately 90% confluency. Tumor cells were labeled by incubating with MPIO-GFP (Bangs lab) for 24 hours and allowed to adhere to the monolayer for 30 minutes. After washing off the nonadherent cells, coverslips were fixed with 4% paraformaldehyde (PFA).

Migration assay

Transwell inserts were coated with 0.2% gelatin (Sigma) for a minimum of 30 minutes and placed in 24-well plate. HBEC cells (4×10^4) were applied to upper chamber of the inserts and allowed to grow for 3 days. Tumor cells were labeled by incubating with MPIO-GFP for 24 hours and applied (4×10^4), seeded on the upper chamber, and incubated for 24 hours. Inserts were washed with PBS, fixed with 4% PFA for 20 minutes, and washed with PBS twice. The inserts were removed from the plate, and nonmigrated cells were scraped off with cotton swabs. Membranes were cut from the inserts, placed the lower side up, and mounted with prolong gold antifade reagent on a microscope slide.

Brain slice assay

After labeling with MPIO-GFP (Bangs lab) for 24 hours, 1×10^5 tumor cells were injected into the left ventricle of mouse hearts. Mice were sacrificed at 1 hour following intracardiac injection, and brains were placed in a dish containing ice-cold Hank's Balanced Salt Solution on ice. Brains were then embedded with 6% agarose gel and placed on ice-cold stainless-steel brain matrices (0.5 mm, Coronal, 40–75 g) before sectioning. Vessels in brains were stained with anti-collagen IV antibody (rabbit, Millipore) followed by Alexa Fluor 555 (red)–conjugated secondary antibodies (Cell Signaling Technology).

Aldefluor assay by fluorescence-activated cell sorting

The ALDEFLUOR kit (StemCell Technologies) was used to isolate populations with high ALDH enzymatic activity according to the manufacturer's protocol via a FACS Aria III (BD Bioscience). Briefly, cells were incubated in ALDEFLUOR assay buffer containing an ALDH substrate (1 μmol/L per 1×10^6 cells) for 30 minutes at RT. Each sample of cells was also stained with 150 μmol/L of diethylaminobenzaldehyde, a specific inhibitor of ALDH, as a negative control.

Animal experiments

All animal experiments were performed at the UAB under an Institutional Animal Care and Use Committee–approved protocol (#20290) in accordance with NIH guidelines. Immunocompromised mice (SCID Beige) were purchased from Charles River. For intracardiac injection, mice were anesthetized with ketamine/xylazine and fixed in place. The needle was inserted into the left ventricle of the heart properly from the under-costal space. When blood was observed pumping into the needle tube, we began to slowly inject the cell solution. Mice were placed on the stage warmed at 37°C until they were fully awake. For intracranial injection, dissociated breast cancer cells were stereotactically injected into the striatum of mice as described (28).

Bioluminescence imaging and MRI

Bioluminescence imaging (BLI) was performed as previously described (26). Mice were injected i.p. with 2.5 mg/100 μL solution of XenoLight D-luciferin (PerkinElmer). The tumor luciferase images were captured using an IVIS 100 imaging system (PerkinElmer) 10 minutes after injection of substrate. We also imaged mice with a 9.4T MRI system, Biospec 94/20 (Bruker). Mice were anesthetized with isoflurane, and temperature was maintained via a heated circulating water system during the studies; respiration was monitored with a system from SA Instruments.

RNA sequencing analysis

Briefly, cDNA libraries for paired end sequencing were prepared using TruSeq Stranded mRNA-Seq Library Preparation Kit (Illumina) according to the manufacturer's protocol. Samples were sequenced with an Illumina HiSeq 2000 system (Illumina), and 100 bp paired-end reads were generated. The raw sequencing and processed data have been submitted to Gene Expression Omnibus with accession number (GSE138361). Sequence reads in fastq format were imported into a local instance of galaxy (galaxy.uabgrid.uab.edu). STAR (version 2.5.3a) was used to align the raw RNA-Seq fastq reads to the human reference genome from Gencode (GRCh38 Release 25; ref. 29).

Gene expression data analysis

Gene set enrichment analysis (GSEA) was performed using available online software (http://software.broadinstitute.org/gsea/index.jsp). Gene Ontology (GO) enrichment analysis also was performed using available website (http://geneontology.org/).

Statistical analyses

Statistical analysis was performed using XLSTAT 2018.5, SPSS statistical package version 25, and Graphpad Prism 7.0 software. All data were presented as the mean ± SD. P values < 0.05 were considered statistically significant. Statistically significant differences in Kaplan–Meier survival curves were determined by the log-rank analysis.

Results

Reduced OS of TNBC BM

To investigate the clinical impact of BCBM in comparison with primary breast cancer and breast cancer metastases to other organs, we performed analyses of patient OS before and after metastasis. Based on the Centers for Disease Control and Prevention (CDC) database (https://gis.cdc.gov/Cancer/USCS/DataViz.html), there has been a rising trend in breast cancer annual incidence; however, annual deaths have markedly decreased (**Fig. 1A**). Five-year survival in breast cancer has also demonstrated a positive trend over the past four decades (Supplementary Fig. S2). Following meta-analysis of clinical data from recent studies, we determined that despite reports of elevated incidence of BCBM in HER-2$^+$ breast cancer (41%), patient OS in HER-2$^+$ BCBM is progressively improving, whereas TNBC BM shows significantly worse prognosis with no observable survival benefit over the past decade (**Fig. 1B**; Supplementary Table S3; refs. 3–5, 30–41). Collectively, these data demonstrate the significant challenges encountered in the clinical application of existing treatment paradigms and in novel therapeutic development for BCBM.

Elevated MES markers in BCBM patient matched brain, lung, and bone metastatic tumors

Recent studies, including our own (24), have identified that epithelial–mesenchymal transition (EMT) of brain tumor cells plays a

Published OnlineFirst March 3, 2020; DOI: 10.1158/1535-7163.MCT-19-0461

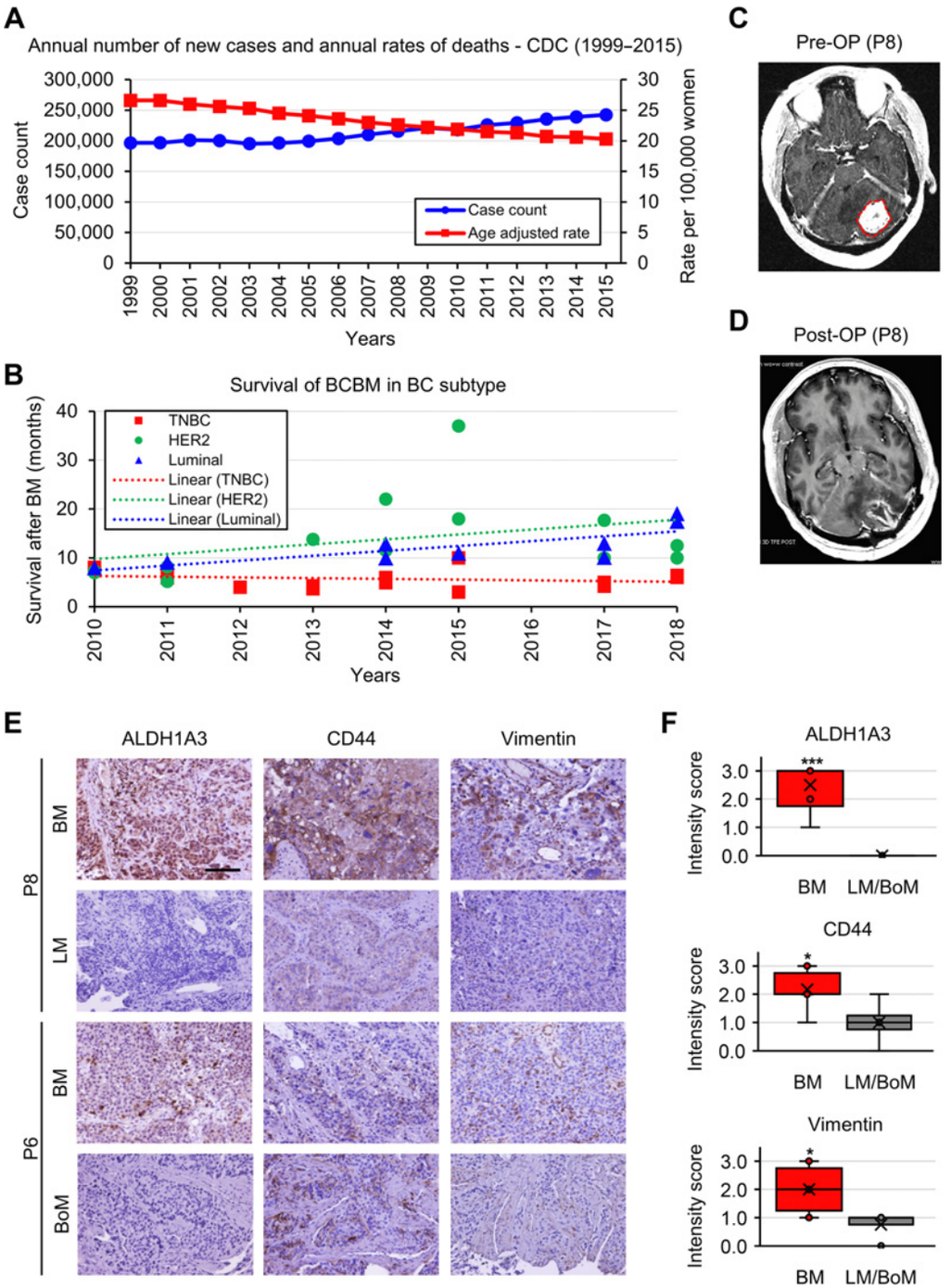

Figure 1.

Mortality, ALDH1A3, and MES marker expressions elevated in BCBM. **A,** Survival analysis of patients with breast cancer based on annual rates of incidence and death from 1999 to 2015, according to the CDC database. **B**, Survival analysis of patients with BCBM comparing OS of TNBC, HER2^{+}, Numinal, and BCBM subtypes from 2006 to 2018, analyzed and compiled from clinical findings of recent peer-reviewed publications (3–5, 30–42). **C,** Representative MRI of BCBM patient 8 (P8) prior to surgical resection of BM. **D,** Postoperative MRI of BCBM P8 following surgical resection of BM. **E,** IHC for ALDH1A3 (left), CD44 (middle), and Vimentin (right) in BM, LM, and BoM in human breast cancer specimens from patients P6 and P8. Scale bar, 100 μm. **F,** Intensity score analysis comparing ALD1A3 (left), CD44 (middle), and Vimentin (right) expressions in BM and LM/BoM. *, $P < 0.05$; ***, $P < 0.001$.

Published OnlineFirst March 3, 2020; DOI: 10.1158/1535-7163.MCT-19-0461

critical role in their malignant transformation and ultimate resistance to therapy. To clarify the relationship between the three EMT-representative proteins (ALDH1A3, CD44, and Vimentin) and BM, we compared their expression in tumor tissue derived from organs which were seeded by breast cancer [i.e., BM, lung metastasis (LM), and bone metastasis (BoM)] of matched patients. None of the patients displayed metastasis to all three organs and as such we compared the expression between either BM and LM (patient 8) or BM and BoM (patient 6); a preoperative MRI displayed findings typical of BM in patient 8, followed by tumor resection (**Fig. 1C** and **D**). IHC staining determined that ALDH1A3 was highly expressed in BM, whereas expression levels of ALDH1A3 were significantly lower in both LM and BoM (**Fig. 1E** and **F**; Supplementary Fig. S3). This trend was, to some extent, observed by IHC for CD44 and Vimentin (**Fig. 1E** and **F**; Supplementary Fig. S3). These findings indicate that breast cancer cells convert to an MES phenotype when metastasizing to the brain, but not lungs or bones, accompanied by strong induction of ALDH1A3 expression.

Elevated ALDH1A3, CD44, and Vimentin expression in BCBM mouse models and BM-forming cell lines

To further evaluate the signature of metastasized breast tumors, we established a metastatic murine model via the cardiac injection of human TNBC cells; MDA-MB-231 (MDA-231) and MDA-MB-468 (MDA-468) using immunocompromised mice (SCID Beige). IHC examining resultant metastatic tumors demonstrated that BMs express ALDH1A3, CD44, and Vimentin at markedly higher levels in comparison with their LM and BoM counterparts (**Fig. 2A**; Supplementary Fig. S4A). These findings indicate that BCBM murine mouse models faithfully recapitulate the ALDH1A3 and MES marker expression previously noted in human BCBM.

From the resultant tumors within the brain, lung, or bone, we produced a series of derivative cell lines and performed RNA sequencing (RNA-seq) of these tumor cells. Subsequent principal component analysis (PCA) of MES gene expression profiles from these derivative lines demonstrated that those cells derived from BM are in fact distinct from primary, LM, and BoM; heatmap analysis of 373 EMT-representative genes does confirm this (**Fig. 2B** and **C**; Supplementary Table S4). We selected 13 genes that overlapped between 373 EMT-representative genes and our 31 MES gene set in GBM and performed qPCR. Note that 231 BM showed different expression pattern and highly expressed ALDH1A3, CD44, and Vimentin as compared with cells obtained from primary and other metastatic sites (**Fig. 2D** and **E**; Supplementary Fig. S4B). Fluorescence-activated cell sorting (FACS) further confirmed elevated ALDH1A3 expression in 231-BM on the cellular level, compared with MDA-231 (**Fig. 2F**; Supplementary Fig. S4C). WB and IF also showed the difference in expression of ALDH1A3 at the protein level (**Fig. 2G** and **H**). CD44 and Vimentin protein levels were consistently higher in BM, supporting the qRT-PCR results (Supplementary Fig. S4D). Collectively, our data indicate that these mouse models of breast cancer–derived metastases faithfully recapitulate the MES phenotype of human disease, further supporting the notion that ALDH1A3 is selectively upregulated in BMs compared with primary lesions and/or other metastases of breast cancers.

ALDH1A3 and CD44 display spatially and temporally distinct expression profiles

Given the elevated expression of the MES markers (ALDH1A3, CD44, and Vimentin) in BM tissues, we sought to determine the intratumoral spatial distribution and temporal change of these markers throughout the course of initiation and propagation of BM tumors. In sharp contrast to CD44 expression, ALDH1A3 expression was noted to a greater extent at the tumor-stromal cell boundary (**Fig. 3A** and **B**; Supplementary Fig. S5).

Of note, the intensity of ALDH1A3 expression was substantially higher at the infiltrating edges compared with the core of the tumor, indicating that ALDH1A3 may play some role in expansion and/or invasion of BM cells into the brain parenchyma (**Fig. 3C**). To evaluate the temporal changes of ALDH1A3 and CD44 expression from the time of colonization to tumor cell expansion, we investigated ALDH1A3 and CD44 expression in the brain at several time points (i.e., 7, 14, and 28 days) following intracardiac injection of MDA-231. IHC revealed that ALDH1A3 expression was detectable as early as 7 days, whereas CD44 expression gradually increased between days 14 and 28 (**Fig. 3D** and **E**). These data suggest that ALDH1A3 may play a role in the early/initial phases of BM formation (i.e., in the transition from circulating breast cancer cells to tumor).

ALDH1A3 plays roles in cell adhesion and migration of circulating breast cancer cells

Because ALDH1A3 is preferentially expressed by BM lesions (**Fig. 1**), we investigated whether ALDH1A3 drives establishment of BM by circulating breast cancer cells. We employed a gene silencing strategy using lentiviral infection with shRNA targeting ALDH1A3 in MDA-231 and MDA-468 cells. qRT-PCR analysis for relative expression of ALDH1A3 in infected MDA-231 and MDA-468 cells confirmed downregulation of ALDH1A3 in these two cell lines (**Fig. 4A**). shRNA-mediated gene silencing of ALDH1A3 resulted in attenuated cell proliferation of MDA-231 and MDA-468 cells (**Fig. 4B**). Comparative analysis for adhesion capacity in shALDH1A3- or shNT-infected MDA-231 and MDA-468 cells demonstrated significantly reduced adhesion ability following ALDH1A3 knockdown (**Fig. 4C**; Supplementary Fig. S6A). Similarly, a migration assay comparing shNT- and shALDH1A3-infected MDA-231 and MDA-468 cells demonstrated significantly reduced migration ability following ALDH1A3 knockdown (**Fig. 4D**; Supplementary Fig. S6B). In line with such findings, GO enrichment analysis comparing sh/siNT or sh/siALDH1A3 MDA-231 cells demonstrated significant downregulation of gene sets associated with cell–cell adhesion, cell junction, and extracellular matrix (**Fig. 4E**). GSEA comparing ECM receptor interaction in sh/siNT- and sh/siALDH1A3-infected MDA-231 cells demonstrated inhibition of this pathway following ALDH1A3 knockdown (**Fig. 4F**). These data strongly suggest that ALDH1A3 plays roles in the cell adhesion and migration of circulating breast cancer cells.

Next, we sought to establish a means of visualizing and monitoring the initial phase of BM formation. To this end, we developed brain slices utilizing mice that received intracardiac injection of GFP-labeled MDA-231 cells. Interestingly, GFP signals were already detected in the capillaries of these mouse brains at 2 hours after intracardiac injection (**Fig. 4G**). For validation of these findings, we performed intracardiac injection of shNT or shALDH1A3 MDA-231 cells labeled with ultrasmall superparamagnetic iron oxide nanoparticles, followed by T1 weighted MRI at 2 hours and 8 days. MRI demonstrated substantially decreased metastatic foci as early as 2 hours and to a lesser extent at 8 days, in the shALDH1A3 group (**Fig. 4H**). Collectively, these data indicate that circulating breast cancer cells rapidly colonize in the brain to form metastases in an ALDH1A3-dependent manner as early as 2 hours following intracardiac injection.

Published OnlineFirst March 3, 2020; DOI: 10.1158/1535-7163.MCT-19-0461

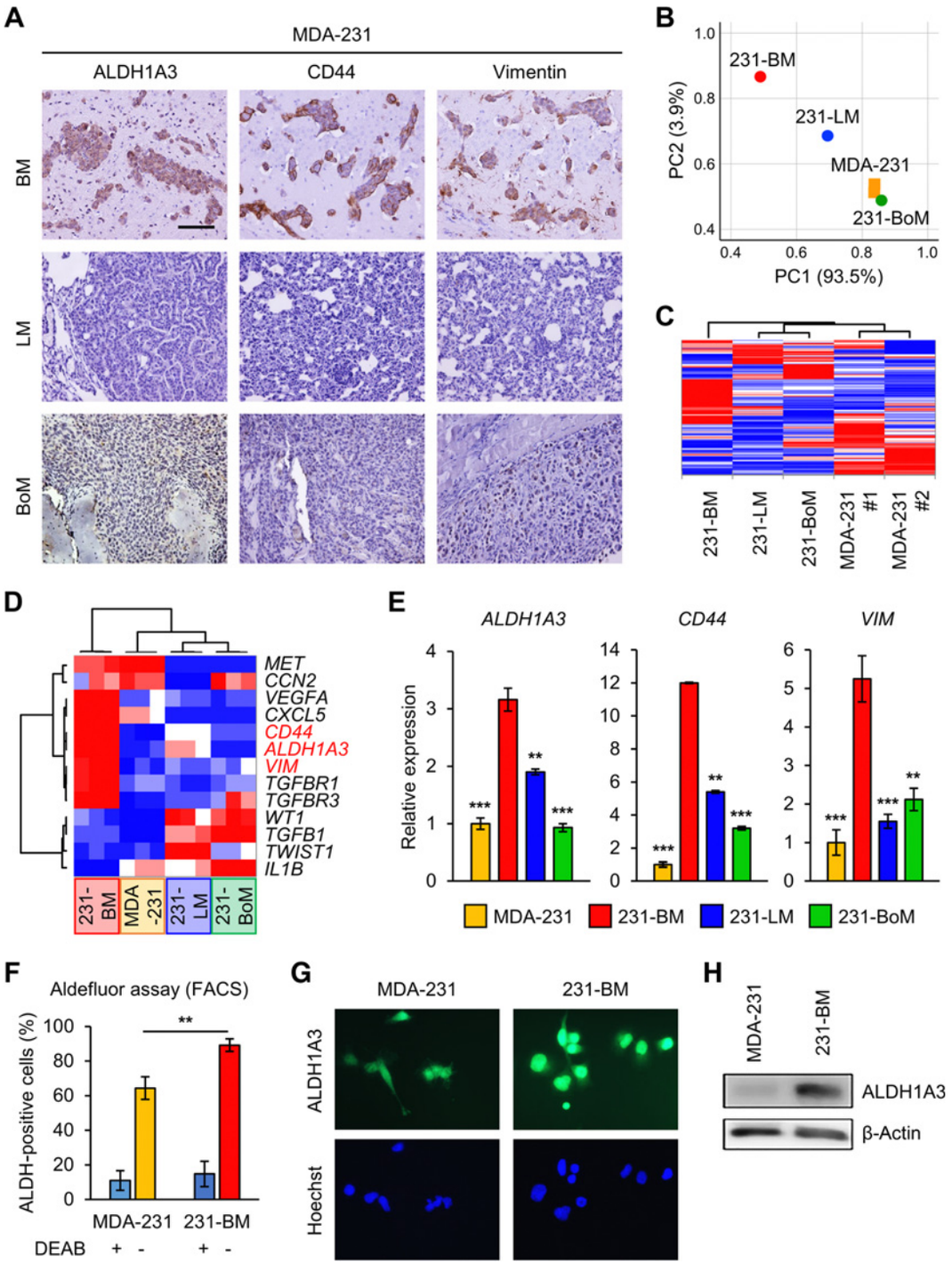

Figure 2.

TNBC xenograft mice models phenocopy expression patterns of human breast cancer metastases. **A,** IHC of mice BM (top), LM (middle), and BoM (bottom) following intracardiac injection of MDA-231 cells for ALDH1A3 (left), CD44 (middle), and Vimentin (right). Scale bar, 100 μm. **B,** PCA of MDA-231 (orange, $n = 2$), 231-BM (red, $n = 1$), 231-LM (blue, $n = 1$), and 231-BoM (green, $n = 1$) cells via RNA-seq. **C,** Clustered heatmap of RNA-seq data in MDA-231 ($n = 2$), 231-BM ($n = 1$), 231-LM ($n = 1$), and 231-BoM ($n = 1$) cells. **D,** Clustered heatmap of qRT-PCR data of 13 MES genes in MDA-231, 231-BM, 231-LM, and 231-BoM cells. **E,** qRT-PCR analysis for expression of *ALDH1A3, CD44*, and *VIM* in MDA-231, 231-BM, 231-LM, and 231-BoM cells. Data are mean ± SD ($n = 3$). **, $P < 0.01$; ***, $P < 0.001$. **F,** FACS comparing ALDH1A3 expression in MDA-231 and 231-BM. Data are mean ± SD ($n = 3$ for DEAB$^+$; $n = 5$ for DEAB$^-$). **, $P < 0.01$. **G,** IF staining for ALDH1A3 expression in MDA-231 and 231-BM cells. Nuclei were counterstained with Hoechst (blue). Scale bar, 20 μm. **H,** WB for ALDH1A3 expression in MDA-231 and 231-BM cells. β-Actin utilized as internal control.

Published OnlineFirst March 3, 2020; DOI: 10.1158/1535-7163.MCT-19-0461

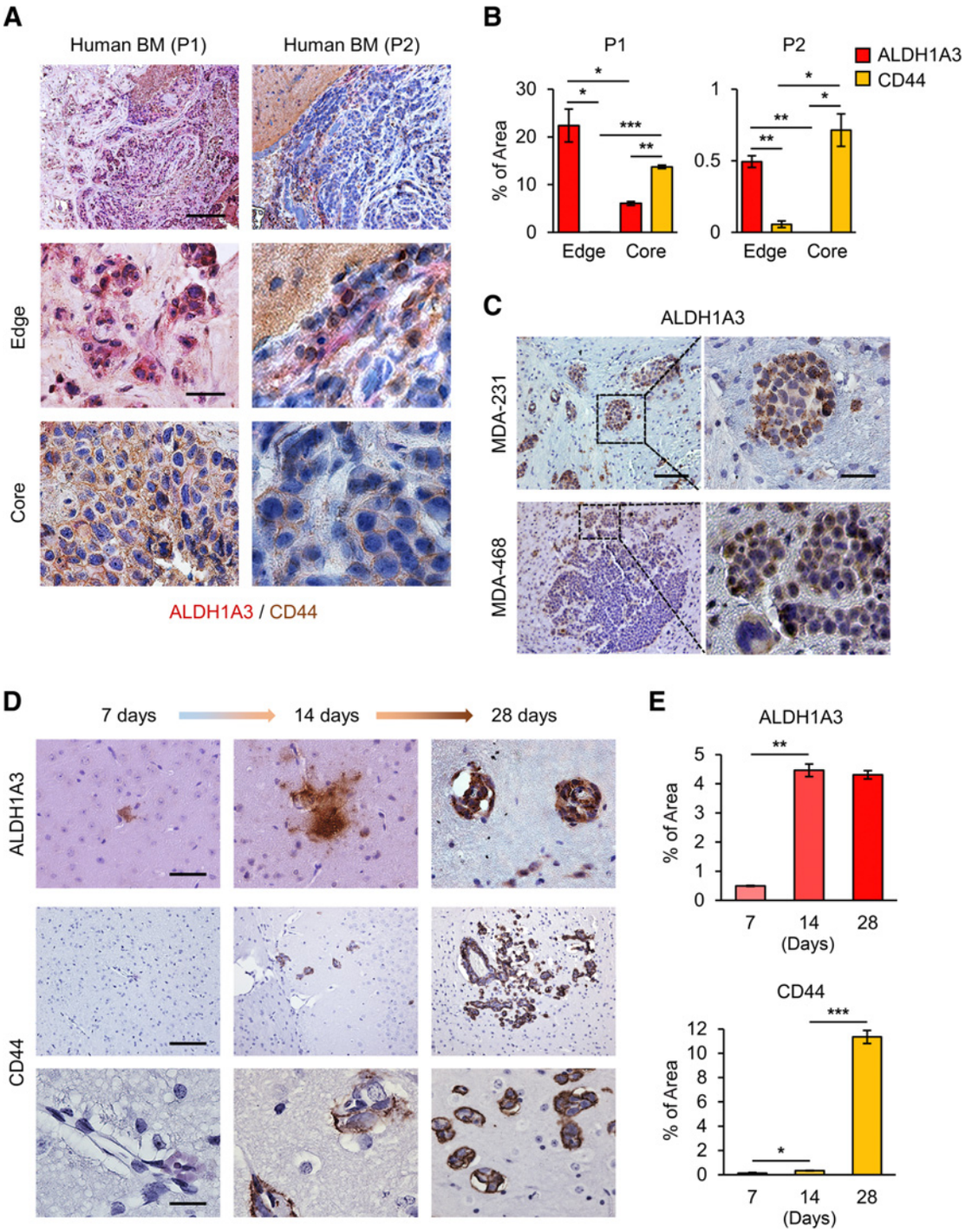

Figure 3.

ALDH1A3 and CD44 display spatially and temporally distinct expression patterns. **A,** IHC of 2 human BCBM patient specimens for ADLH1A3 expression (red) and CD44 expression (brown) at the tumor-stromal cell boundary (middle) and tumor core (lower). Scale bars, 200 μm (top) and 20 μm (middle and bottom). **B,** Percentage of stained area of ALDH1A3 and CD44 in **A**. Data are mean ± SD ($n = 3$). *, $P < 0.05$; **, $P < 0.01$; and ***, $P < 0.001$. **C,** IHC of mice brains following intracardiac injection of MDA-231 or MDA-468 cells for ADLH1A3 expression (red). Scale bars, 200 μm (left) and 20 μm (right). **D,** IHC of mice brains following intracardiac injection of MDA-231 cells at 7 (left), 14 (middle), and 28 (right) days for CD44 (top) and ALDH1A3 (bottom). Scale bars, 100 μm (top) and 20 μm (middle and bottom). **E,** Percentage of stained area of ALDH1A3 (top) and CD44 (bottom) in Fig. 3D. Data are mean ± SD ($n = 3$). *, $P < 0.05$; **, $P < 0.01$; and ***, $P < 0.001$.

Published OnlineFirst March 3, 2020; DOI: 10.1158/1535-7163.MCT-19-0461

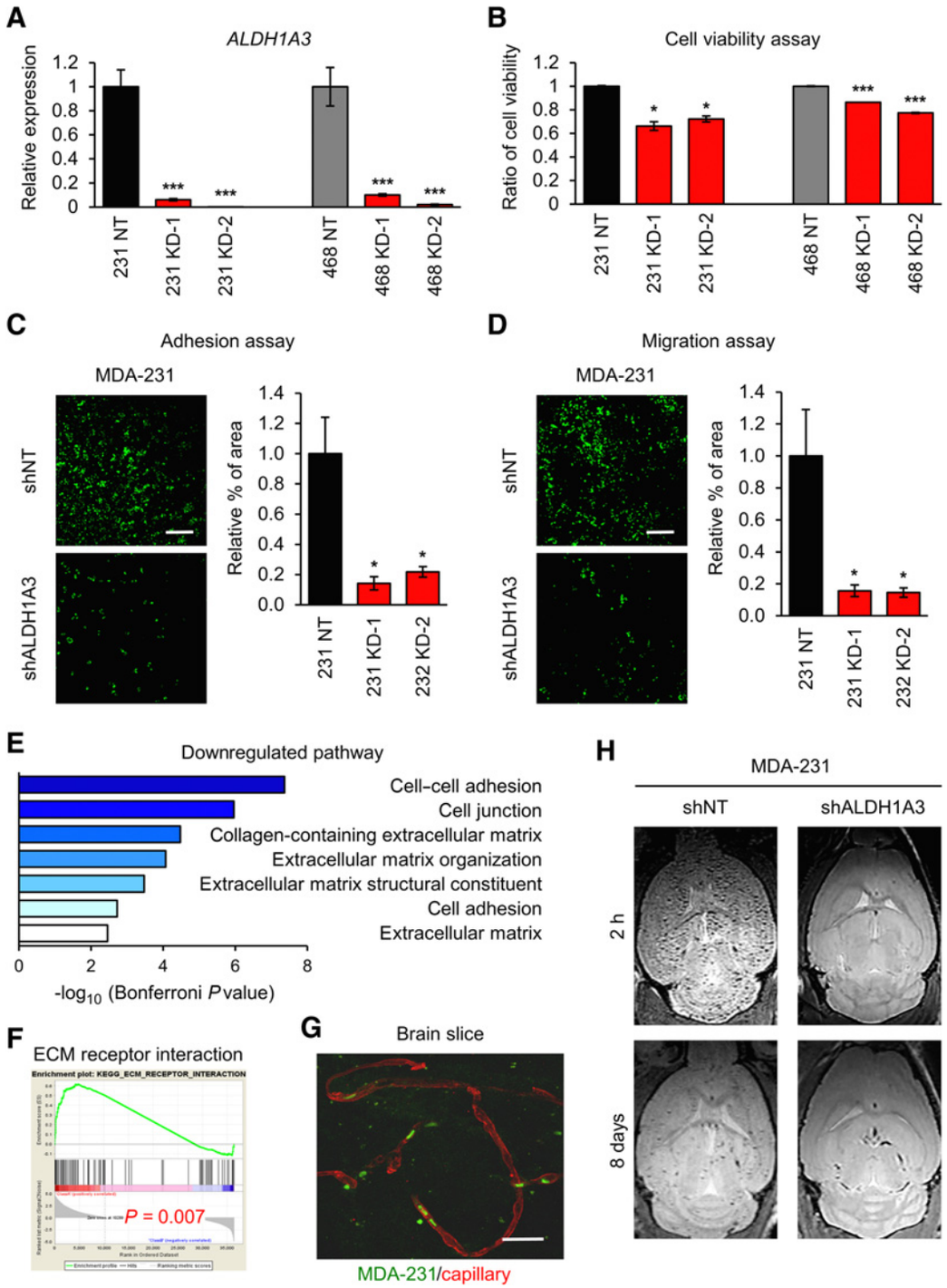

Figure 4.

Role of ALDH1A3 in adhesion and migration of CTCs. **A,** qRT-PCR analysis for the expression of *ALDH1A3* in MDA-231 and MDA-468 cells expressing siNT, siALDH1A3_1, or siALDH1A3_2. Data are mean ± SD ($n = 3$). ***, $P < 0.001$. **B,** Cell viability assay of shNT (left) or siALDH1A3 (right) infected MDA-231 cells. Data are mean ± SD ($n = 5$ for shNT; $n = 3$ for shALDH1A3). *, $P < 0.05$; ***, $P < 0.001$. **C,** Adhesion assay of shNT (top) or shALDH1A3 (bottom) infected MDA-231 cells. Cells labeled with GFP (green). Data are mean ± SD ($n = 4$). *, $P < 0.05$. **D,** Migration assay of shNT (top) or shALDH1A3 (bottom) infected MDA-231 cells. Cells labeled with GFP (green). Data are mean ± SD ($n = 4$). *, $P < 0.05$. **E,** GO ontology pathway analyses of RNA-seq data for comparison between shNT and shALDH1A3 MDA-231 cells. **F,** GSEA comparing ECM receptor interaction pathway in siNT- or siALDH1A3-infected MDA-231 cells. $P = 0.007$. **G,** Mouse brain slice culture demonstrating MDA-231 cell (GFP, green) preferential proximity to vasculature (Collagen IV, red). **H,** T1 weighted MRI of mice brains following intracardiac injection of MDA-231–incubated MPIO with shNT or shALDH1A3 at 2 hours (top) and 8 days (bottom).

Published OnlineFirst March 3, 2020; DOI: 10.1158/1535-7163.MCT-19-0461

Genetic inhibition of ALDH1A3 decreases initiation of BM in murine models

Next, we sought to explore the function/phenotype of ALDH1A3 in BCBM. To this end, we employed a gene silencing strategy using lentiviral transduction of shRNA targeting ALDH1A3 (shALDH1A3) in MDA-231 cells. BLI revealed that shALDH1A3 knockdown in MDA-231 cells prior to intracardiac injection significantly reduced the frequency and size of BM compared with nontargeting shRNA (shNT) control (**Fig. 5A**). Hematoxylin and eosin (H&E) staining of brain slices from these two groups of mice showed that BM formation was substantially diminished upon ALDH1A3 knockdown (**Fig. 5B**). Suppression of ALDH1A3 expression by shRNA infection was confirmed in all three organs with metastatic tumors, although basal levels of ALDH1A3 expression in LM and BoM were markedly lower than that in BM (**Fig. 5C**). Interestingly, shALDH1A3 also diminished CD44 and Vimentin expression in BM, reinforcing that ALDH1A3 may promote the expression of MES markers during the initiation phase of BCBM (**Fig. 5D**). Collectively, these findings support a role for ALDH1A3 during BM initiation and MES phenotype development, without an appreciable effect on LM and BoM formation.

To investigate the BM-specific effect of shALDH1A3, we compared the outcome of intracardiac and intracranial injection of MDA-231 and MDA-468 cells. BLI showed that intracardiac injection leads to the formation of all metastases: BM, LM, and BoM, whereas intracranial injection led to no metastases (**Fig. 5E**). In brains, small and multiple BM foci were observed in the intracardiac injection model, whereas intracranial injection formed larger, solitary tumors (**Fig. 5E** and **F**). As expected, ALDH1A3 knockdown significantly prolonged survival following intracardiac injection of both MDA-231 and MDA-468 (**Fig. 5G**; Supplementary Fig. S7A). In contrast, the impact of ALDH1A3 knockdown on the survival of these tumor-bearing mice with intracranial injection was less pronounced (**Fig. 5H**; Supplementary Fig. S7B). These results indicate the essential yet not exclusive role of ALDH1A3 with regard to initial phases of circulating breast cancer cells establishing BM formation.

ALDH1A3 inhibitor MF-7 prolongs survival and intercepts BM formation

To evaluate ALDH1A3 targeting as a potential therapeutic strategy in BCBM, we utilized a medicinal chemistry approach to develop a novel small molecule that binds to and inhibits the activity of ALDH1A3. We modified the imidazo [1,2-*a*] pyridine hit GA11, which we previously described as an effective ALDH1A3 inhibitor, by inserting a fluoro substituent in the para position of the 6-phenyl ring (**Fig. 6A**; ref. 42). The resultant compound, MF-7, fully preserved the inhibitory activity of the imidazo [1,2-*a*] pyridine class compound against the target protein when tested in a cell-free assay performed on recombinant human ALDH1A3 (IC_{50} 22.8±1.6 μmol/L for MF-7 vs. IC_{50} 4.7±1.7 μmol/L for GA11; Supplementary Fig. S1; Supplementary Table S1), but displayed a significantly increased functional efficacy, compared with GA11, when tested for antiproliferative activity in the MDA-468 cell line; log-dose analysis indicates enhanced response in comparison with NH32, MF-6, and GA11 (**Fig. 6B**; Supplementary Fig. S8A). Collectively, these findings indicate target engagement of the novel ALDH1A3 inhibitor (MF-7) and cytotoxicity against breast cancer cells *in vitro*.

To evaluate *in vivo*, we intraperitoneally administered MF-7 in mice for 8 consecutive days before and after intracardiac injection of MDA-231 and MDA-468 cells (**Fig. 6C**). This treatment protocol did not cause adverse reactions in the treated mice, yet significantly prolonged their survival compared with the DMSO control group (**Fig. 6D**). H&E staining of brain slices demonstrated formation of smaller and fewer BM tumors in the MF-7–treated mice compared with the control (**Fig. 6E**). As expected, the levels of CD44 expression in the MF-7–treated tumors were reduced compared with the control group (**Fig. 6F**). Surprisingly, and in sharp contrast to the effect on BM formation, the numbers of LM or BoM were paradoxically higher in the MF-7 group as compared with the DMSO group (**Fig. 6G** and **H**). We posited that the susceptibility of increased frequency of LM and BoM may be related to alteration of the target organ following inhibition of ALDH1A3 activity. This hypothesis may be explained due to single-cell RNA-seq (scRNA-seq) which determined that ALDH1A3 expression was elevated in normal brain endothelial cells, whereas in the normal lung, ALDH1A3 expression was elevated in fibroblasts (Supplementary Fig. S8B and S8C), indicating variance of ALDH1A3 expression in normal vascular endothelial cells of the target organs (i.e., brain, lung). Collectively, these results suggest that ALDH1A3 inhibition is selectively effective in suppressing BM, but not metastases to other organs (i.e., lung, bone).

Discussion

Herein, we have highlighted current clinical challenges surrounding the management of BCBM, which is underscored by a lack of recent prognostic and therapeutic advancements in the setting of TNBC. We also sought to clarify the molecular signature associated with BCBM (6–8), and in so doing identified key roles for ALDH1A3 and genes previously associated with EMT. We determined that ALDH1A3 expression is selectively elevated in human BCBM, a finding that is recapitulated by BM cell cultures *in vitro* as well as the tumors established after BM xenografts *in vivo*. Further, our data suggest that elevated expression of ALDH1A3 precedes other MES markers (e.g., CD44) during the early phase of BM formation. We demonstrated that ALDH1A3 plays roles in the initiation and cell adhesion phases in the BM developmentary cascade, but not LM and BoM. Genetic inhibition of ALDH1A3 via lentiviral shRNA led to significant survival benefit in BCBM mouse models (56% intracardiac, 32% intracranial). Beside our data, other recent findings reveal organ-specific enhancement of metastasis and unique gene signature expression using multiple sublines derived from BM, LM, and BoM of the parental cell line MDA-MB-231 (43, 44). In BM, ST6GALNAC5 was reported as key molecule to enhance CTC's adhesion to brain endothelial cells and their passage through BBB (6). In addition, SLITRK2, TMEM47, and LYPD1 were identified as upregulated genes in BM compared with LM and BoM (45).

The ALDH superfamily is a group of nicotinamide adenine dinucleotide NAD or $NADP^+$-dependent enzymes acting as the primary aldehyde metabolic system in human cells (46). Of note, the level of ALDH enzymatic activity has been used as a CSC marker and seemingly correlates with tumor aggressiveness (47, 48). ALDH1A3 is abnormally expressed in various cancers and CSCs, including breast cancer (49–51). Marcato and colleagues reported that ALDH1A3 is strongly expressed in poorly differentiated and metastatic late-stage breast cancer patients (48), whereas other studies have highlighted the role of ALDH1A3 expression in patients with TNBC which correlates with clinical stage (52, 53). Our prior study determined that ALDH1A3 expression was higher in GBM's aggressive subtype of glioma stem cells (24). Together, ALDH1A3 as CSC-associated enzyme is a mediator of tumorigenicity, metastasis, and therapy resistance as is the case with CSC-associated signaling pathways such as Notch, Wnt, and Hedgehog (54). In melanoma, ALDH1A3 knockout by siRNA significantly decreased the expression of melanoma stem cell–related genes

Published OnlineFirst March 3, 2020; DOI: 10.1158/1535-7163.MCT-19-0461

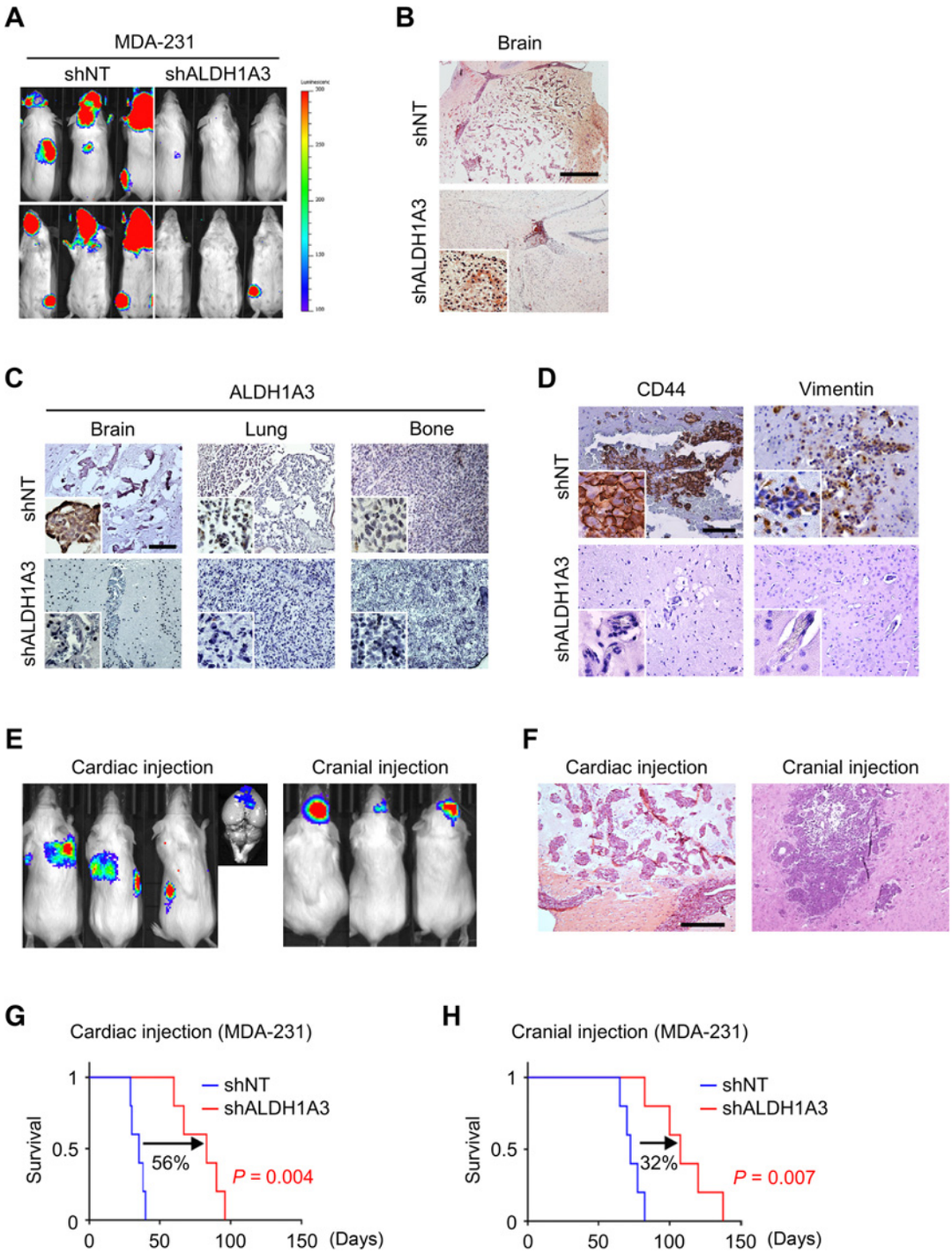

Figure 5.

Genetic inhibition of ALDH1A3 decreases initiation of BM and prolongs survival. **A,** BLI of mice 1 month after intracardiac injection of luciferase-labeled shNT- or shALDH1A3-infected MDA-231 cells. **B,** Representative H&E staining of mouse brain following intracardiac injection of shNT- (top) or shALDH1A3 (bottom)-infected MDA-231 cells. Scale bar, 500 μm. **C,** Representative IHC for ALDH1A3 in BM (left), LM (middle), and BoM (right) in mice following intracardiac injection of shNT- (top) or shALDH1A3 (bottom)-infected MDA-231 cells. Scale bar, 100 μm. **D,** Representative IHC for CD44 (left) and Vimentin (right) in BM of mice following intracardiac injection of shNT- (top) or shALDH1A3 (bottom)-infected MDA-231 cells. Scale bars, 100 μm. **E,** BLI of mice 1 month after intracardiac (left) and intracranial (right) injection of shALDH1A3 MDA-231 cells. **F,** Representative H&E staining of mouse brain following intracardiac (left) and intracranial (right) injection of shALDH1A3 MDA-231 cells. **G,** Kaplan–Meier survival analysis of mice following intracardiac injection of shNT and shALDH1A3 MDA-231 cells. **H,** Kaplan–Meier survival analysis of mice following intracranial injection of shNT and shALDH1A3 MDA-231 cells.

Published OnlineFirst March 3, 2020; DOI: 10.1158/1535-7163.MCT-19-0461

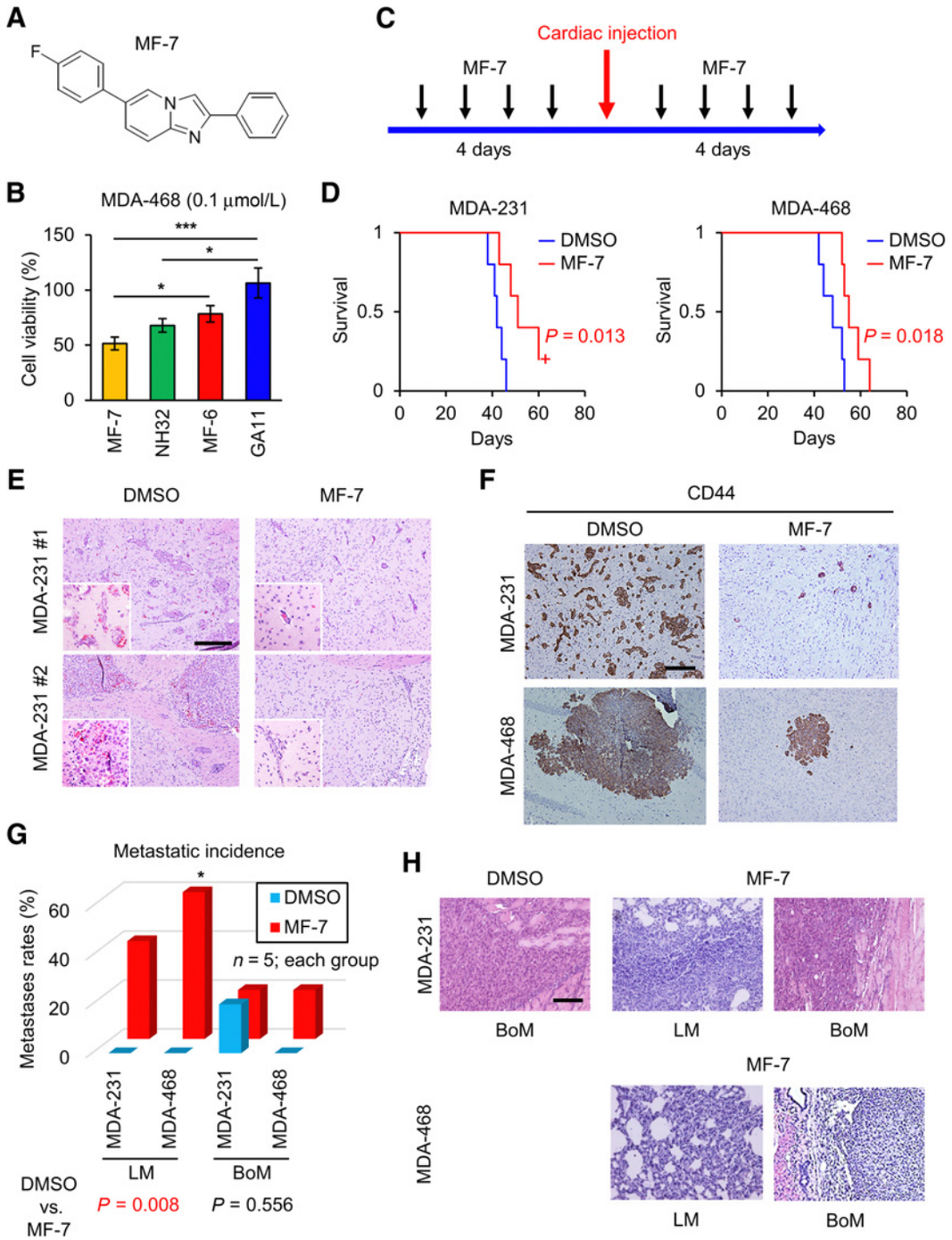

Figure 6.

Interception of BM formation by ALDH1A3 inhibitor MF-7 with survival benefit. **A,** Chemical structure of the ALDH inhibitor GA11 and its analog, MF-7. **B,** Bar graph comparing log-dose response analyses of ALDH1A3 inhibitor MF-7, NH32, MF-6, and GA11 based on cell viability assay of MDA-468 cells. *, $P < 0.05$; ***, $P < 0.001$. **C,** Schematic representation of MF-7 administration prior to and following intracardiac injection of MDA-231 or MDA-468 cells. **D,** Kaplan–Meier survival analyses of mice following intracardiac injection of MDA-231 (left) or MDA-468 (right) cells and treatment with DMSO or MF-7. $P = 0.013$ and 0.018 respectively. **E,** Representative H&E staining of mice BM following intracardiac injection of MDA-231 cells. Mice were treated with DMSO (left) or MF-7 (right) before and after intracardiac injection. Scale bar, 100 μm. **F,** Representative IHC for CD44 in BM of mice treated with DMSO (left) or MF-7 (right) before and after intracardiac injection of MDA-231 cells. Scale bar, 100 μm. **G,** Bar graph comparing frequency of LM or BoM in mice treated with DMSO or MF-7 before and after intracardiac injection of MDA-231 or MDA-468 cells. $n = 5$ each. *, $P < 0.05$. **H,** H&E staining of LM and BoM of mice treated with DMSO (left) or MF-7 (middle, right) before and after intracardiac injection of MDA-231 or MDA-468 cells. Scale bar, 100 μm.

Published OnlineFirst March 3, 2020; DOI: 10.1158/1535-7163.MCT-19-0461

such as CDC42 and USH1C (55). Despite this, ALDH1A3 has yet to be evaluated in BM.

Previously, we had determined that ALDH1A3 plays a role in GBM's PN–MES transition (24). Here, our findings indicate that ALDH1A3 plays roles in CTC adherence to brain vascular endothelial cells and extravasation into brain parenchyma. In addition, the inhibition of ALDH1A3 prolonged xenograft mice survival following both intracardiac and intracranial injection of TNBC cells, albeit to a lesser degree by the latter. Given the antitumor formation effects of ALDH1A3 inhibition in intracranial injection models, it is likely that ALDH1A3′s function involves a multistep process in BCBM which may include effects related to our prior findings in GBM. These data raise the possibility that elevated cancer cell ALDH1A3 activity provides an advantage with regard to both survival and progression of cancer cells within the brain. Future investigations will seek to fully elucidate the mechanisms underlying ALDH1A3′s effects, and in doing determine whether ALDH1A3 is responsible for a shared role in both primary and metastatic CNS cancers.

Our findings suggest significant therapeutic benefit via application of MF-7 for both primary prevention of BCBM in patients with breast cancer and post-BCBM establishment. However, one side-effect of MF-7 administration in intracardiac injection models was elevated susceptibility with regard to LM and BoM formation, which may be related to alteration of the target organs by circulating breast cancer cells following inhibition of ALDH1A3 activity. Although the survival of intracardiac injection models following MF-7 administration exhibited an overall increase (∼20%), suggesting a positive trade-off in cost-benefit, it remains to be seen whether similar findings will be observed in humans. In addition, comparisons in patient quality of life would ultimately be required to assess potential improvement due to reduced BM formation versus reduced LM and BoM. Given that ALDH1A3 expression is elevated in normal endothelial cells of the brain (Supplementary Fig. S7A), likely similar targeting mechanisms may be employed to reduce metastases formation in other organs. Recently studies reported that citral is an effective ALDH1A3 inhibitor to block ALDH1A3-mediated BC growth (54) and that NRAD1 targeting therapy has the potential for the treatment of TNBC and the reduction of CSCs (56). These will be points of interest to be discerned by future BCBM preclinical studies and clinical trials.

Several recently developed therapeutics are under investigation for BCBM; however, the $HER2^+$ phenotype of BCBM has dominated recent clinical trials (57–59), potentially owing to increased frequency of $HER2^+$ BCBM. Systemic modalities including manipulation of the BBB allowing for delivery of traditional chemotherapeutics, novel chemotherapeutics (e.g., etirinotecan pegol, peptide–paclitaxel conjugates), novel targeted therapies (e.g., pan-HER receptor and CDK4/6 inhibitors), PARP inhibitors, and immunotherapies are all under investigation by preclinical and clinical studies (60). Given the lack of therapeutic modalities with appreciable efficacy in TNBC BM, targeting ALDH1A3 may prove an effective option in this intractable disease. Beyond BCBM, the inhibition of ALDH1A3-mediated pathways may ultimately provide a promising therapeutic approach for cancers displaying MES and/or stem-like signatures (e.g., aggressive subsets of GBM; refs. 24, 61). Interestingly, ALDH1A3 expression in human GBM has been correlated with a worse prognosis and is associated with resistance against Temozolomide treatment with sensitivity to the drug having been re-established in ALDH1A3 knockout cells (62). Accordingly, a number of strategies have begun to emerge that seek to target ALDH1A3 isoforms ranging from immunotherapy (63) to traditional small-molecule–based approaches (64).

Conclusion

In this study, we highlighted a lack of appreciable improvement in OS of TNBC BM over the past two decades. We demonstrated novel roles for ALDH1A3 during the cell migration and adhesion phases of the metastatic cascade in BCBM, but not LM or BoM. Targeting ALDH1A3 proved to be effective via both genetic and pharmacologic inhibition. Our findings present ALDH1A3 as an attractive target for primary prevention and therapeutic management of BCBM, suggest applicability of similar metastasis-guiding molecules to other cancers beyond TNBC, and provide a rationale for the therapeutic targeting of ALDH1A3 in a broader context. The identification of ALDH1A3-specific inhibitors may create a new paradigm for development of targeted therapeutics for BCBM and other metastatic carcinomas.

Disclosure of Potential Conflicts of Interest

J.D. Bernstock has an ownership interest (including patents) in CITC Ltd. and Avidea Technologies, and has an unpaid consultant/advisory board relationship with POCKiT Diagnostics. No potential conflicts of interest were disclosed by the other authors.

Authors' Contributions

Conception and design: I. Nakano
Development of methodology: D. Yamashita, M. Minata, V. Coviello, B.A. Tannous, I. Nakano
Acquisition of data (provided animals, acquired and managed patients, provided facilities, etc.): D. Yamashita, M. Minata, S. Yamaguchi, S. Harada, C. La Motta
Analysis and interpretation of data (e.g., statistical analysis, biostatistics, computational analysis): D. Yamashita, M. Minata, S. Yamaguchi, V. Coviello, J.D. Bernstock, S. Harada, B.A. Tannous, C. La Motta
Writing, review, and/or revision of the manuscript: D. Yamashita, A.N. Ibrahim, J.D. Bernstock, S. Harada, B.A. Tannous, C. La Motta, I. Nakano
Study supervision: R.A. Cerione, I. Nakano

Acknowledgments

The authors wish to thank Dr. Amdra R. Frost (UAB) for MDA-MB-468.

This study was supported by the NIH grants R01NS083767, R01NS087913, R01CA183991, and R01CA201402 (I. Nakano).

The costs of publication of this article were defrayed in part by the payment of page charges. This article must therefore be hereby marked *advertisement* in accordance with 18 U.S.C. Section 1734 solely to indicate this fact.

Received May 1, 2019; revised October 3, 2019; accepted February 25, 2020; published first March 3, 2020.

References

1. Waks AG, Winer EP. Breast cancer treatment: a review. JAMA 2019;321:288–300.
2. Kodack DP, Askoxylakis V, Ferraro GB, Fukumura D, Jain RK. Emerging strategies for treating brain metastases from breast cancer. Cancer Cell 2015;27:163–75.
3. Kim YJ, Kim JS, Kim IA. Molecular subtype predicts incidence and prognosis of brain metastasis from breast cancer in SEER database. J Cancer Res Clin Oncol 2018;144:1803–16.
4. Niikura N, Hayashi N, Masuda N, Takashima S, Nakamura R, Watanabe K, et al. Treatment outcomes and prognostic factors for patients with brain metastases

from breast cancer of each subtype: a multicenter retrospective analysis. Breast Cancer Res Treat 2014;147:103–12.
5. Tseng LM, Hsu NC, Chen SC, Lu YS, Lin CH, Chang DY, et al. Distant metastasis in triple-negative breast cancer. Neoplasma 2013;60:290–4.
6. Bos PD, Zhang XH, Nadal C, Shu W, Gomis RR, Nguyen DX, et al. Genes that mediate breast cancer metastasis to the brain. Nature 2009;459:1005–9.
7. Lee JY, Park K, Lee E, Ahn T, Jung HH, Lim SH, et al. Gene expression profiling of breast cancer brain metastasis. Sci Rep 2016;6:28623.
8. Klein A, Olendrowitz C, Schmutzler R, Hampl J, Schlag PM, Maass N, et al. Identification of brain- and bone-specific breast cancer metastasis genes. Cancer Lett 2009;276:212–20.
9. Valiente M, Obenauf AC, Jin X, Chen Q, Zhang XH, Lee DJ, et al. Serpins promote cancer cell survival and vascular co-option in brain metastasis. Cell 2014;156:1002–16.
10. Leone JP, Leone BA. Breast cancer brain metastases: the last frontier. Exp Hematol Oncol 2015;4:33.
11. DiStefano A, Yong Yap Y, Hortobagyi GN, Blumenschein GR. The natural history of breast cancer patients with brain metastases. Cancer 1979;44: 1913–8.
12. Rostami R, Mittal S, Rostami P, Tavassoli F, Jabbari B. Brain metastasis in breast cancer: a comprehensive literature review. J Neurooncol 2016;127:407–14.
13. Brastianos PK, Carter SL, Santagata S, Cahill DP, Taylor-Weiner A, Jones RT, et al. Genomic characterization of brain metastases reveals branched evolution and potential therapeutic targets. Cancer Discov 2015;5:1164–77.
14. Pedrosa R, Mustafa DA, Soffietti R, Kros JM. Breast cancer brain metastasis: molecular mechanisms and directions for treatment. Neuro Oncol 2018;20: 1439–49.
15. Custodio-Santos T, Videira M, Brito MA. Brain metastasization of breast cancer. Biochim Biophys Acta Rev Cancer 2017;1868:132–47.
16. Kienast Y, von Baumgarten L, Fuhrmann M, Klinkert WE, Goldbrunner R, Herms J, et al. Real-time imaging reveals the single steps of brain metastasis formation. Nat Med 2010;16:116–22.
17. Follain G, Osmani N, Azevedo AS, Allio G, Mercier L, Karreman MA, et al. Hemodynamic forces tune the arrest, adhesion, and extravasation of circulating tumor cells. Dev Cell 2018;45:33–52.
18. Chen Q, Boire A, Jin X, Valiente M, Er EE, Lopez-Soto A, et al. Carcinoma-astrocyte gap junctions promote brain metastasis by cGAMP transfer. Nature 2016;533:493–8.
19. Li F, Tiede B, Massague J, Kang Y. Beyond tumorigenesis: cancer stem cells in metastasis. Cell Res 2007;17:3–14.
20. Charafe-Jauffret E, Ginestier C, Iovino F, Wicinski J, Cervera N, Finetti P, et al. Breast cancer cell lines contain functional cancer stem cells with metastatic capacity and a distinct molecular signature. Cancer Res 2009;69:1302–13.
21. Ginestier C, Hur MH, Charafe-Jauffret E, Monville F, Dutcher J, Brown M, et al. ALDH1 is a marker of normal and malignant human mammary stem cells and a predictor of poor clinical outcome. Cell Stem Cell 2007;1:555–67.
22. Badve S, Nakshatri H. Breast-cancer stem cells-beyond semantics. Lancet Oncol 2012;13:e43–8.
23. DA Cruz Paula A, Lopes C. Implications of different cancer stem cell phenotypes in breast cancer. Anticancer Res 2017;37:2173–83.
24. Mao P, Joshi K, Li J, Kim SH, Li P, Santana-Santos L, et al. Mesenchymal glioma stem cells are maintained by activated glycolytic metabolism involving aldehyde dehydrogenase 1A3. Proc Natl Acad Sci U S A 2013;110:8644–9.
25. Cheng P, Phillips E, Kim SH, Taylor D, Hielscher T, Puccio L, et al. Kinome-wide shRNA screen identifies the receptor tyrosine kinase AXL as a key regulator for mesenchymal glioblastoma stem-like cells. Stem Cell Reports 2015;4:899–913.
26. Pavlyukov MS, Yu H, Bastola S, Minata M, Shender VO, Lee Y, et al. Apoptotic cell-derived extracellular vesicles promote malignancy of glioblastoma via intercellular transfer of splicing factors. Cancer Cell 2018;34:119–35.
27. Wang J, Cheng P, Pavlyukov MS, Yu H, Zhang Z, Kim SH, et al. Targeting NEK2 attenuates glioblastoma growth and radioresistance by destabilizing histone methyltransferase EZH2. J Clin Invest 2017;127:3075–89.
28. Nakano I, Joshi K, Visnyei K, Hu B, Watanabe M, Lam D, et al. Siomycin A targets brain tumor stem cells partially through a MELK-mediated pathway. Neuro Oncol 2011;13:622–34.
29. Dobin A, Davis CA, Schlesinger F, Drenkow J, Zaleski C, Jha S, et al. STAR: ultrafast universal RNA-seq aligner. Bioinformatics 2013;29:15–21.
30. Arslan UY, Oksuzoglu B, Aksoy S, Harputluoglu H, Turker I, Ozisik Y, et al. Breast cancer subtypes and outcomes of central nervous system metastases. Breast 2011;20:562–7.
31. Bai B, Yuan ZY, Liu DG, Teng XY, Wang SS. Clinical features and survival analysis of different subtypes of patients with breast cancer brain metastases. Chin J Cancer 2010;29:413–9.
32. Fokas E, Henzel M, Hamm K, Grund S, Engenhart-Cabillic R. Brain metastases in breast cancer: analysis of the role of HER2 status and treatment in the outcome of 94 patients. Tumori 2012;98:768–74.
33. Honda Y, Aruga T, Yamashita T, Miyamoto H, Horiguchi K, Kitagawa D, et al. Prolonged survival after diagnosis of brain metastasis from breast cancer: contributing factors and treatment implications. Jpn J Clin Oncol 2015;45: 713–8.
34. Jang G, Lee SS, Ahn JH, Jung KH, Lee H, Gong G, et al. Clinical features and course of brain metastases in triple-negative breast cancer: comparison with human epidermal growth factor receptor 2-positive and other type at single institution in Korea. Breast Cancer Res Treat 2011; 128:171–7.
35. Jeon W, Jang BS, Jeon SH, Kim JH, Kim YJ, Kim SH, et al. Analysis of survival outcomes based on molecular subtypes in breast cancer brain metastases: a single institutional cohort. Breast J 2018;24:920–6.
36. Kuba S, Ishida M, Nakamura Y, Yamanouchi K, Minami S, Taguchi K, et al. Treatment and prognosis of breast cancer patients with brain metastases according to intrinsic subtype. Jpn J Clin Oncol 2014;44:1025–31.
37. Kwon HC, Oh SY, Kim SH, Lee S, Kwon KA, Choi YJ, et al. Clinical outcomes and breast cancer subtypes in patients with brain metastases. Onkologie 2010;33: 146–52.
38. Matsuo S, Watanabe J, Mitsuya K, Hayashi N, Nakasu Y, Hayashi M. Brain metastasis in patients with metastatic breast cancer in the real world: a single-institution, retrospective review of 12-year follow-up. Breast Cancer Res Treat 2017;162:169–79.
39. Oehrlich NE, Spineli LM, Papendorf F, Park-Simon TW. Clinical outcome of brain metastases differs significantly among breast cancer subtypes. Oncol Lett 2017;14:194–200.
40. Shen Q, Sahin AA, Hess KR, Suki D, Aldape KD, Sawaya R, et al. Breast cancer with brain metastases: clinicopathologic features, survival, and paired biomarker analysis. Oncologist 2015;20:466–73.
41. Tarhan MO, Demir L, Somali I, Yigit S, Erten C, Alacacioglu A, et al. The clinicopathological evaluation of the breast cancer patients with brain metastases: predictors of survival. Clin Exp Metastasis 2013;30: 201–13.
42. Cheng P, Wang J, Waghmare I, Sartini S, Coviello V, Zhang Z, et al. FOXD1-ALDH1A3 signaling is a determinant for the self-renewal and tumorigenicity of mesenchymal glioma stem cells. Cancer Res 2016;76:7219–30.
43. Lu X, Yan CH, Yuan M, Wei Y, Hu G, Kang Y. In vivo dynamics and distinct functions of hypoxia in primary tumor growth and organotropic metastasis of breast cancer. Cancer Res 2010;70:3905–14.
44. Lu X, Lu X, Kang Y. Organ-specific enhancement of metastasis by spontaneous ploidy duplication and cell size enlargement. Cell Res 2010;20:1012–22.
45. Burnett RM, Craven KE, Krishnamurthy P, Goswami CP, Badve S, Crooks P, et al. Organ-specific adaptive signaling pathway activation in metastatic breast cancer cells. Oncotarget 2015;6:12682–96.
46. Vasiliou V, Nebert DW. Analysis and update of the human aldehyde dehydrogenase (ALDH) gene family. Hum Genomics 2005;2:138–43.
47. Liu S, Ginestier C, Ou SJ, Clouthier SG, Patel SH, Monville F, et al. Breast cancer stem cells are regulated by mesenchymal stem cells through cytokine networks. Cancer Res 2011;71:614–24.
48. Marcato P, Dean CA, Liu RZ, Coyle KM, Bydoun M, Wallace M, et al. Aldehyde dehydrogenase 1A3 influences breast cancer progression via differential retinoic acid signaling. Mol Oncol 2015;9:17–31.
49. Duan JJ, Cai J, Guo YF, Bian XW, Yu SC. ALDH1A3, a metabolic target for cancer diagnosis and therapy. Int J Cancer 2016;139:965–75.
50. Kurth I, Hein L, Mabert K, Peitzsch C, Koi L, Cojoc M, et al. Cancer stem cell related markers of radioresistance in head and neck squamous cell carcinoma. Oncotarget 2015;6:34494–509.
51. Marcato P, Dean CA, Pan D, Araslanova R, Gillis M, Joshi M, et al. Aldehyde dehydrogenase activity of breast cancer stem cells is primarily due to isoform ALDH1A3 and its expression is predictive of metastasis. Stem Cells 2011;29: 32–45.
52. Opdenaker LM, Arnold KM, Pohlig RT, Padmanabhan JS, Flynn DC, Sims-Mourtada J. Immunohistochemical analysis of aldehyde dehydrogenase isoforms and their association with estrogen-receptor status and disease progression in breast cancer. Breast Cancer 2014;6:205–9.

Published OnlineFirst March 3, 2020; DOI: 10.1158/1535-7163.MCT-19-0461

53. Ali HR, Dawson SJ, Blows FM, Provenzano E, Pharoah PD, Caldas C. Cancer stem cell markers in breast cancer: pathological, clinical and prognostic significance. Breast Cancer Res 2011;13:R118.
54. Thomas ML, de Antueno R, Coyle KM, Sultan M, Cruickshank BM, Giacomantonio MA, et al. Citral reduces breast tumor growth by inhibiting the cancer stem cell marker ALDH1A3. Mol Oncol 2016;10:1485–96.
55. Luo Y, Dallaglio K, Chen Y, Robinson WA, Robinson SE, McCarter MD, et al. ALDH1A isozymes are markers of human melanoma stem cells and potential therapeutic targets. Stem Cells 2012;30:2100–13.
56. Vidovic D, Huynh TT, Konda P, Dean C, Cruickshank BM, Sultan M, et al. ALDH1A3-regulated long non-coding RNA NRAD1 is a potential novel target for triple-negative breast tumors and cancer stem cells. Cell Death Differ 2020;27:363–78.
57. Lin NU, Dieras V, Paul D, Lossignol D, Christodoulou C, Stemmler HJ, et al. Multicenter phase II study of lapatinib in patients with brain metastases from HER2-positive breast cancer. Clin Cancer Res 2009;15:1452–9.
58. Van Swearingen AED, Siegel MB, Deal AM, Sambade MJ, Hoyle A, Hayes DN, et al. LCCC 1025: a phase II study of everolimus, trastuzumab, and vinorelbine to treat progressive HER2-positive breast cancer brain metastases. Breast Cancer Res Treat 2018;171:637–48.
59. Freedman RA, Gelman RS, Wefel JS, Melisko ME, Hess KR, Connolly RM, et al. Translational breast cancer research consortium (TBCRC) 022: a phase II trial of neratinib for patients with human epidermal growth factor receptor 2-positive breast cancer and brain metastases. J Clin Oncol 2016;34:945–52.
60. Kotecki N, Lefranc F, Devriendt D, Awada A. Therapy of breast cancer brain metastases: challenges, emerging treatments and perspectives. Ther Adv Med Oncol 2018;10:1758835918780312.
61. Nakano I. Stem cell signature in glioblastoma: therapeutic development for a moving target. J Neurosurg 2015;122:324–30.
62. Wu W, Schecker J, Wurstle S, Schneider F, Schonfelder M, Schlegel J. Aldehyde dehydrogenase 1A3 (ALDH1A3) is regulated by autophagy in human glioblastoma cells. Cancer Lett 2018;417:112–23.
63. Visus C, Wang Y, Lozano-Leon A, Ferris RL, Silver S, Szczepanski MJ, et al. Targeting ALDH(bright) human carcinoma-initiating cells with ALDH1A1-specific CD8(+) T cells. Clin Cancer Res 2011;17:6174–84.
64. Koppaka V, Thompson DC, Chen Y, Ellermann M, Nicolaou KC, Juvonen RO, et al. Aldehyde dehydrogenase inhibitors: a comprehensive review of the pharmacology, mechanism of action, substrate specificity, and clinical application. Pharmacol Rev 2012;64:520–39.

Published OnlineFirst March 3, 2020; DOI: 10.1158/1535-7163.MCT-19-0461

Molecular Cancer Therapeutics

Identification of ALDH1A3 as a Viable Therapeutic Target in Breast Cancer Metastasis–Initiating Cells

Daisuke Yamashita, Mutsuko Minata, Ahmed N. Ibrahim, et al.

Mol Cancer Ther 2020;19:1134-1147. Published OnlineFirst March 3, 2020.